An overview of DLR compound rotorcraft aerodynamics and aeroacoustics activities within the CleanSky2 NACOR Project

*Marc Wentrup
Research Scientist

*Jianping Yin
Research Scientist

*Philipp Kunze
Research Scientist

*Thomas Streit
Research Scientist

*Jan-Hendrik Wendisch
Research Scientist

*Thorsten Schwarz
Head of the helicopter department

*(DLR Braunschweig, Germany)

+Jean-Paul Pinacho
Engineer

+Klaus Kicker
Engineer

+Raphaël Fukari
Engineer

+(Airbus Helicopters, France)

ABSTRACT

The challenge of increasing range and speed of a rotorcraft is encountered in the scope of the European CleanSky2 "Fast Rotorcraft" project by Airbus Helicopters with the compound helicopter design RACER (RapidAndCostEfficientRotorcraft) for which the box wing and the tail parts designs are respectively protected by patent. This paper presents the DLR contributions to the RACER development. This includes the aerodynamic design of the wing and tail section as well as an overall assessment of performance and noise. In a first step the aerodynamic properties of the configuration are evaluated both isolated and with consideration of the main rotor and lateral rotor interferences by the use of actuator discs. In the second step, the investigated possibilities to improve the configurations performance are described. These include airfoil design for improved high lift performance of the wing and tail section, an optimization of the box wing circulation distribution on the upper and lower wing. Additionally, the intersection fairings were improved and the efficiency of the trim flaps was evaluated. In this regard, it could be determined for which cases an isolated approach is appropriate and when the rotor interference should be considered. At the end the evaluation of the aero acoustics of the configuration is conducted. The applied configuration shows good aerodynamic characteristics with some further cruise and off design optimization potential.

NOTATION

AC	Aircraft mode
AD	Actuator disc
AH	Airbus Helicopters
AoA	Angle of attack
C_L	Lift coefficient
c_l	Local lift coefficient
C_D	Drag coefficient
c_d	Local drag coefficient
e	Spanwise efficiency factor
HC	Helicopter mode
HS	Horizontal stabilizer
L/D	Lift to drag ratio
LR	Lateral rotors
LW	Lower wing
LWFJ	Lower wing/fuselage junction
LWNJ	Lower wing/nacelle junction
MR	Main rotor
TB	Tail boom
TPS	Thin plate splines
UW	Upper wing
UWFJ	upper wing/fuselage junction
UWNJ	upper wing/nacelle junction
VF	vertical fin

INTRODUCTION

At high speed, the main rotor of a helicopter faces the problems of low velocity flow condition on the retreating blade and high velocity conditions on the advancing blade. The first problem leads to large reverse flow regions and high angle of attack, causing high drag due to flow separations. The second one goes along with compressibility effects, increasing noise and wave drag. These problems aggravate with rising cruise speed and disc loading. For a conventional helicopter, the disc loading results from the requirement to provide the necessary lift force to keep the aircraft in the air as well as the thrust component to overcome the resulting drag force of the aircraft.

Within the European CleanSky2 project "Fast Rotorcraft", with support from the parallel CleanSky2 project "Airframe", Airbus Helicopters (AH) answers this challenge with its RACER (RapidAndCostEfficientRotorcraft) configuration, designated to travel at cruise speeds around 400km/h (220kts). The design consists of a mid-weight

Presented at the AHS International 74th Annual Forum & Technology Display, Phoenix, Arizona, USA, May 14-17, 2018.

helicopter with a staggered box wing, attached to the fuselage. The wing is designated to share the lift generation with the main rotor (MR) to decrease its loading. Additionally, two lateral rotors (LR) in pusher configuration are installed at the wing tips to relieve the main rotor from thrust generation. Thus the main rotor is further unloaded, enabling faster and more efficient cruise flight.

The activities presented in this paper were carried out jointly with ONERA as part of a call for tender won in the ITD AIRFRAME of the CleanSky 2 platform. ONERA contributed to the design of the lateral rotors, and the vertical fins (VF), whilst the acoustic analysis is being carried out jointly by DLR and ONERA. The DLR was in charge of the aerodynamic design of the wing, and of the horizontal stabilizer (HS) (see Figure 1). The particularity of the project was to work on each component individually, taking into account the many aerodynamic interactions between wing/LR, LR/wing, MR/LR/wing/tail parts, requiring numerous and frequent exchanges between the partners.

Due to the vast amount of activities, this paper is focused on the aerodynamic activities contributed by DLR (wing and horizontal stabilizer design), presented in four sections. First the configuration is described. After this the aerodynamic characteristics are analyzed. This is done for the configuration without rotors and additionally with the consideration of the rotor interferences to identify the interaction effects. After gaining experience with regards to the aerodynamic characteristics, several approaches for improving the design are evaluated for the wing and for the horizontal stabilizer. These efforts targeted to improve cruise flight performance by airfoil design as well as optimization of the circulation distribution and the aerodynamics for the junctions. This was specially challenging as the boundary conditions constantly changed during the development. This is due to the ongoing progression in other disciplines like structural design and system integration for example, which were carried out in parallel. At the end, the evaluation of the aeroacoustics properties of the configuration is presented.

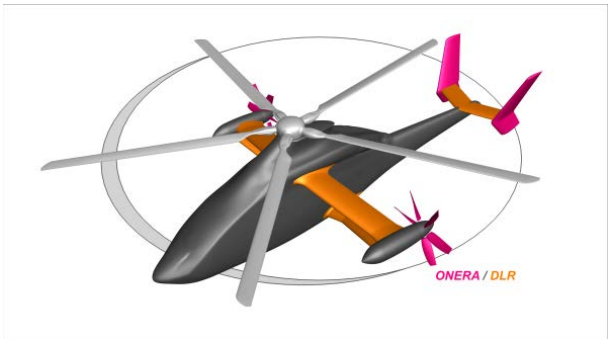

Figure 1 illustration of DLR and ONERA workshare

DESCRIPTION OF THE CONFIGURATION

Figure 2 shows the configuration design of the RACER, with a box wing arrangement and an H-shape empennage. The box wing section consists of an upper wing (UW) part which is connected by the nacelles at the tip with the lower wing part (LW). The upper wing orientation is defined by the lateral rotor driving shaft which is hosted inside this wing. It provides a negative sweep angle and an anhedral angle to connect the main gear box with the lateral rotors. The spanwise chord distribution is constant and has been chosen by a tradeoff between minimizing the down-wash surface in hover and low relative thickness of the airfoil. The lower wing (LW) is divided into two parts. The inboard part hosts the landing gear which defines the planform of this part. Therefore a large wing root is required to provide enough space. In spanwise direction the inboard part is tapered to match the shorter chord length of the outboard part. As the rear landing gear position has to be located behind the center of gravity the outboard section of the lower wing has a positive sweep angle to connect the inboard part with the nacelle. The dihedral of the outboard lower wing is defined by a trade-off between interference effects of the upper and lower wing at the wing tip, the parasite drag of non-lifting surfaces and structure weight as discussed in [1]. The resulting dihedral of the wing outer part does not match the angle of the inboard part, forming a kink at the intersection. The upper wings as well as the outboard lower wings are equipped with flaps to adapt the wings lift to different trim conditions and to cancel the lift during autorotation to provide enough flow feeding in the rotor plane.

For the empennage design an H-tail architecture was selected by AH during a wind tunnel test campaign. The box wing configuration shows to have good pitch moment properties, enabling a relatively small horizontal stabilizer surface. The yaw stability requirements however require installing a large vertical fin (VF) surface. The empennage is equipped with trim flaps on the horizontal stabilizer as well as on the vertical fins.

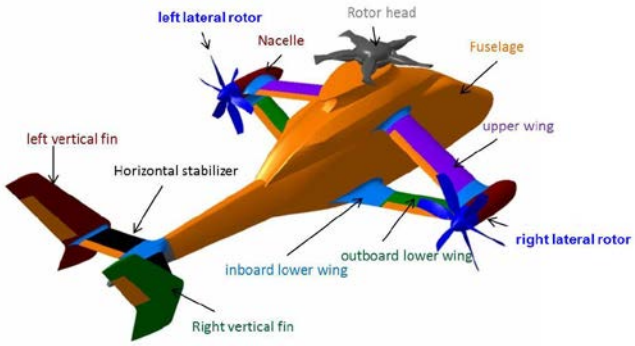

Figure 2 RACER configuration

EVALUATION OF AERODYNAMIC CHARACTERISTICS WITHOUT ROTOR INTERACTION

For the completely new configuration design it was necessary to get a general understanding of the aerodynamic characteristics of the different components and their interaction. In a first attempt the wing and tail section were investigated without consideration of the main rotor and lateral rotor interaction. Therefore the DLR CFD-solver

TAU, as presented in [2] and [3], was used to compute the isolated configuration in steady state mode. The focus of these investigations was set on the wing section, consisting of the upper wing, the lower wing and the nacelle as well as on the empennage, consisting of the end part of the tail boom, the horizontal stabilizer and the vertical fins. The chapter will start with a short description of the computational setup. Next the general characteristics of the configuration in cruise flight are presented for varying pitch angles, followed by the effect of laminar/turbulent transition on the aerodynamic properties.

Computational setup

The DLR-TAU-code solves the Reynolds-averaged-Navier-Stokes equation (RANS) on a cell vertex, finite volume formulation. For the spatial discretization a central Jameson scheme with matrix dissipation is applied. Time integration is performed with an implicit backward Euler scheme, using LU-SGS. During the majority of the investigation a two equation k-ω turbulence model, as proposed by [4], was used.

General characteristics

In Figure 3 the lift over AoA curves of the different wing components (left) and tail section parts (right) are presented. The upper wing contribution to the wing section lift is higher compared to the lower wing. As the upper wing is located further forward than the lower wing, the induced velocities cause a reduction of the lower wing effective AoA, while the lower wing induces an augmentation of the upper wing effective AoA. This causes the observed differences in the lift/alpha slope. At high AoA the upper wing starts to stall first which is beneficial for the aircraft stability as a backing pitch moment occurs due to the frontal position of the upper wing. At the same AoA the lower wing also generates a small drop in the lift/alpha slope. This is caused by a local separation at the transition kink from the inboard to the outboard part of the wing. The initial design shows an overall good aerodynamic performance meeting most requirements. The demanded lift to drag ratio (L/D) of the wing section was almost reached while the maximum lift had to be further improved in order to meet the requirements.

The empennage downforce is dominated by the horizontal stabilizer contribution, while the vertical fins, due to their dihedral, also produce a small downforce (see Figure 3. At higher AoA the lift/alpha slope gets steeper while it becomes flatter towards negative AoA. This is caused by the stalled inboard lower wing wake hitting the horizontal stabilizer. For negative AoA an increasing interaction with the upper decks wake reduces the horizontal stabilizer efficiency until the wake passes underneath it, resulting in a jump of the downward force. It should also be reminded here that the computations were conducted with a fixed rotor head. Therefore these observations should be considered with caution towards a realistic empennage behavior. It was assumed that the qualitative improvement gain on this simplified model could be transfered to the real rotorcraft behavior. A dedicated investigation of the rotor head wake on the empennage was done by ONERA.

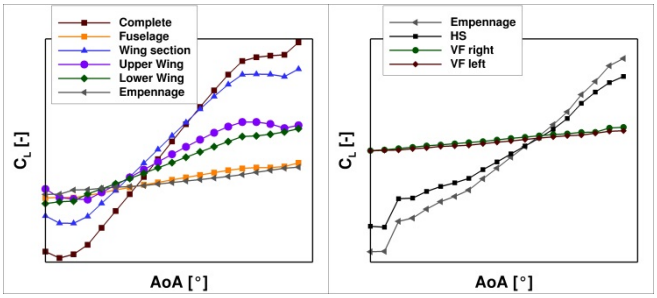

Figure 3 C_L over AoA for the for the wing and tail components without rotor interaction

In Figure 4 the circulation distribution of the wing section is plotted at cruise flight conditions. The lift increases in spanwise direction on the upper wing, before reducing toward the wing tip. Hereby the highest lift occurs at the middle of this wing part. On the lower wing the distribution consists of two local maxima at the kink between inner and outer wing and at the tip while a minimum is formed at the middle of the outboard component. The local maximum at the kink is caused by the increased dihedral of the outer part. In the formed corner, the suction areas of the inboard and outboard section are projected on each other, generating a concentrated suction region. The abrupt lift drop on the upper wing and the lift rise on the lower wing tip are caused by the channeling effect. The flow is accelerated due to the displacement of the bottom side of the upper wing airfoil and the suction side of the lower wing airfoil. The resulting low pressure area sucks the wings towards each other.

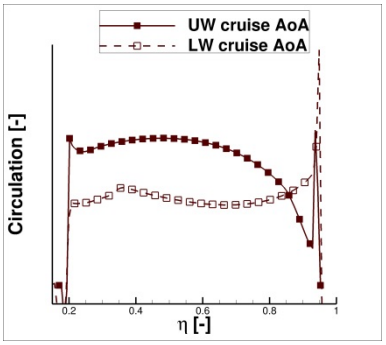

Figure 4 Circulation distributions on UW and LW at cruise AoA without rotor interaction

Laminar/Turbulent transition (wing and tail)

An estimation of the impact of a laminar/turbulent boundary layer for all lifting surfaces was investigated. Therefore the RANS computations with TAU are coupled with the boundary layer code COCO and evaluated by the stability solver LILO as described in [6]. The evaluation is done at cruise flight conditions with constant lift of the configuration as well as for higher AoA to investigate the effect of the boundary layer transition on the maximum lift. In cruise flight conditions, the configurations drag is reduced by about

5.1% at equal lift. In Figure 5 the lift over AoA curve for the case with and without transition prediction is plotted. It can be seen that with transition a higher maximum lift is enabled. When considering the transition, the turbulent boundary layer in the trailing edge region is thinner and consequently less susceptible towards flow separation.

However, the subsequent evaluations and optimizations of the configuration were performed assuming a completely turbulent boundary layer. It was decided that this assumption is the more conservative approach as up to now it is not clear if a natural laminar boundary condition can be realized on the lifting surfaces. Especially the influence of the different noise sources as well as the impact of vibration, mentioned in [5], remain unknown for this configuration as these effects were not addressed during this project.

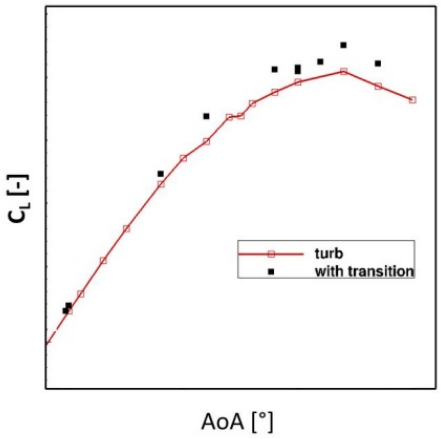

Figure 5 C_L over AoA of the configuration with (black dots) and without (red) laminar flow transition without rotor interaction

EVALUATION OF AERODYNAMIC CHARACTERISTICS WITH ROTOR INTERACTION

A major interest for a compound helicopter is the interaction of the rotors with the different components, in particular the wing section and the empennage. For this purpose the actuator disc (AD) boundary condition of the TAU-code was used. A time constant load distribution is thus prescribed in the rotor disc. This enables to simulate the time averaged induced flow of the rotor in less expensive steady state computations. The load distribution for the main rotor actuator disc was generated by the comprehensive rotor code HOST, as presented by [7]. For the lateral rotors the load distributions were either provided by the unsteady panel method code UPM, presented in [8][9][10] or by the unsteady free-wake method for aerodynamics code PUMA, developed by ONERA and based on the theory described in [11]. The authors of [12] show that this approach gives adequate results for fuselage aerodynamic with main rotor impact. The main rotor head was included during the computations as fixed part.

This chapter will start with description of the hover flight state, followed by the effects during transition flight and finish with the rotor interaction during cruise flight.

Hover

During hover flight the main rotor downwash interacts with the surfaces underneath, causing a downward pointing force on them. It could be confirmed that the wing section adds a major additional amount of the downforce to the fuselage. Due to the box wing design this negative effect could be reduced as the lower wing is shaded by the upper one. Figure 6 shows the breakdown of the relative downforce on the upper and lower wing, referred to the complete wing section. The lower wings amount is reduced to about 25%. Due to the opposite thrust generation of the lateral rotors for anti-torque the download forces on the left and right side differs. The right lateral rotor whose wake passes through the wings even causes a small positive lift force on the right lower wing.

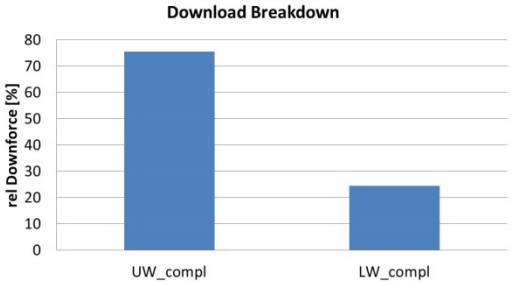

Figure 6 relative downforce breakdown in hover

Hover/cruise flight transition

The transition phase between hover and cruise flight is of special interest for the stability and handling properties of a rotorcraft. Therefore the configuration was computed in a range of different low speed flight velocities to investigate the main and lateral rotor interaction on the components.

The corresponding flow fields in a constant y-plane are plotted in Figure 7. The downforce on the wings first starts to increase at low cruise speeds, before it starts to decrease until it turns into a lift force. The reason for this progression is a combination of two effects. First, the main rotor down-wash consists in an inhomogeneous velocity field which hits the wing section at different positions, depending on the deviation by the free stream velocity. Second, the superposition of the main rotor down-wash and the freestream causes a negative effective pitch angle for the wings. With rising cruise speed, this angle is reduced till it turns positive for higher cruise speed. At smaller negative effective AoA, the flow on the wings reattaches, first causing an increased downforce, until the effective pitch angle enables a positive lift force.

On the empennage the downforce also first increases with rising flow velocity. This is caused by the higher loaded rear section of the main rotor wake which is deflected towards the horizontal stabilizer. While the less accelerated flow of

the main rotor center is deflected on the empennage, the downforce on the horizontal stabilizer decreases, until the higher velocities of the front section of the rotor disc cause again an augmentation.

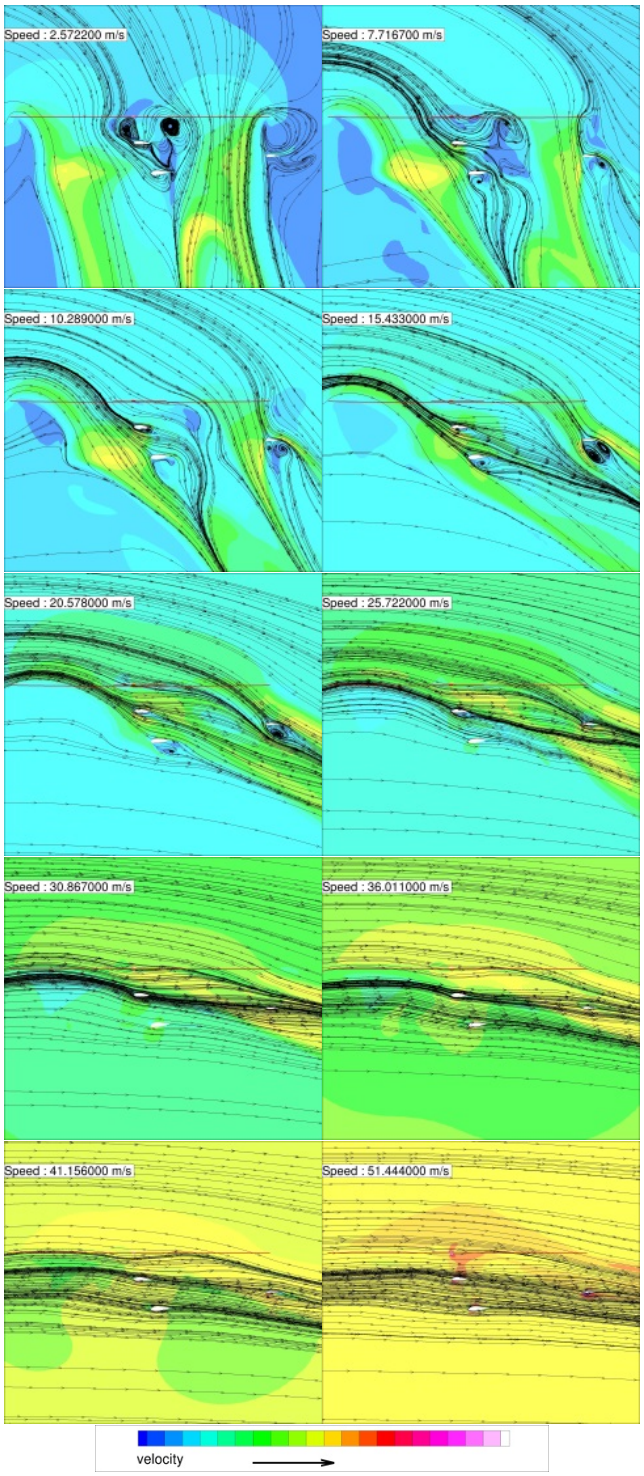

Figure 7 Flow velocity field on wing and horizontal stabilizer at constant y-plane for the configuration with rotor interaction for transition flight

Complete configuration in cruise flight

The complete configuration was additionally recomputed with fully modelled lateral rotors while the main rotor interaction is still modeled by an actuator disc boundary condition (see Figure 8). This was done with prescribed lateral rotor blade pitch settings for three AoA with different wing flap setting angles. The considered cases are summarized in Table 1.

Table 1. Considered cases for complete configuration with resolved LR

cases	AoA [°]	Flap setting [°]
Case 1	-2	7
Case 2	0	0
Case 3	2	-7

The lateral rotors rotation direction was set to counter rotate with respect to the wing tip vortex direction. This means that the right lateral rotor turns in clockwise direction (view from behind) while the left lateral rotor rotates in counter clock wise direction (view from behind). Thus it is possible to improve the lateral rotor efficiency by taking advantage of the swirl recovery from the wing tip vortex. A more detailed explanation of the effects is given in [13].

The negative flap setting angle at AoA=2° results in the fact that Case 3 returns lower lift on the upper wing and lower wing, while the positive setting angle for AoA=-2° generates the highest lift. The corresponding circulation distributions are shown in Figure 9 and Figure 10. For the upper wing and lower wing the characteristic shape previously observed in Figure 4 without rotor influence is still present for AoA=0°. By consideration of the main rotor down-wash, the right wing produces more lift than the left one for all three cases. The lower wing is less affected compared to the upper wing. The effect is caused by the asymmetrical main rotor disc loading, presented in Figure 11. The advancing blade produces a highly loaded area above the left wing position. On the right side the retreating blade is not able to produce significant thrust, so that even a negative loading can be observed in the region above the wing. To trim the rotor, the advancing blade tips have to be negatively loaded while the required main rotor lift is mainly generated by the front and rear disc section. For AoA=±2° the change in the load distribution of the main rotor are minor.

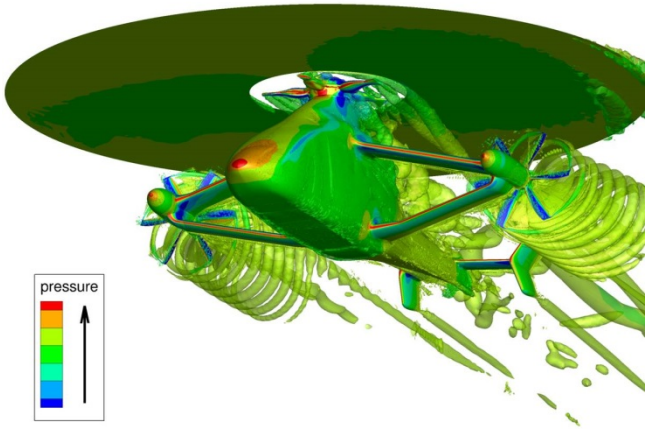

Figure 8 Complete configuration with MR AD and fully modeled lateral rotors

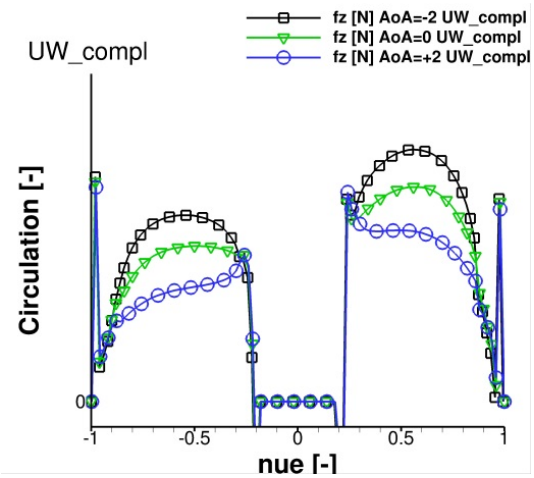

Figure 9 Average circulation distribution on the upper wing for AoA=-2°, AoA=0° and AoA=2° with resolved LR and MR interaction

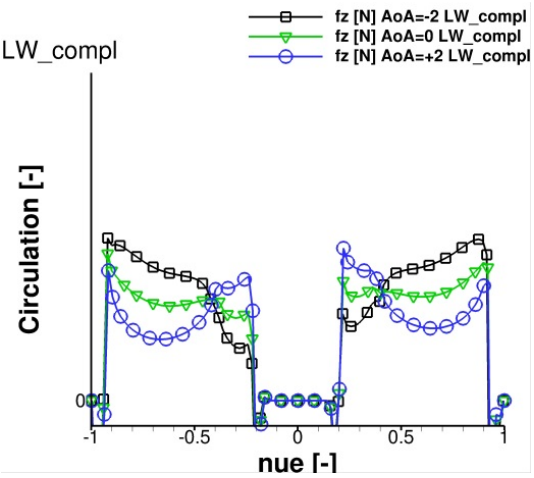

Figure 10 Average circulation distribution on the lower wing for AoA=-2°, AoA=0° and AoA=2° with resolved LR and MR interaction

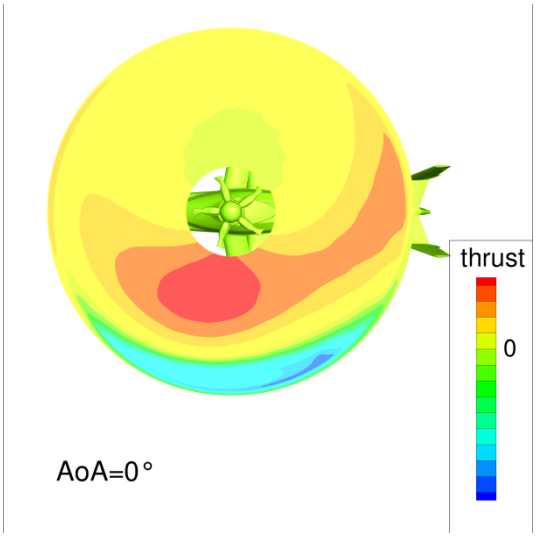

Figure 11 thrust distribution of the MR for AoA=0 with resolved LR and MR interaction

With increasing wing circulation, the lateral rotor thrust as well as the resulting efficiency increases with unchanged blade pitch setting, as it can be observed in Figure 12. This is due to the interaction with the induced velocities of the wing. In Figure 13 the thrust distributions of the lateral rotors for the three cases are plotted. At this point it is interesting to observe that the maximum thrust behind the wing section is higher on the left side, though the right wing produces more lift. The reason is that the main rotor down-wash component that reduces the effective pitch angle on the left wing simultaneously increases the effective pitch angle on the lateral rotor. In Figure 14 the z-component of the velocity is shown in a constant x-plane right in front of the lateral rotors. Due to the counter clock wise rotation direction of the left lateral rotor the upstroking blade is located at the inboard side, facing a high negative z-velocity caused by the main rotor down-wash. However the right lateral rotor generates an overall higher thrust. This is due to the higher pitch setting angle on the right side for yaw control. Additionally, the stronger wing tip vortex causes a higher effective pitch angle on the downstroking blade of right lateral rotor.

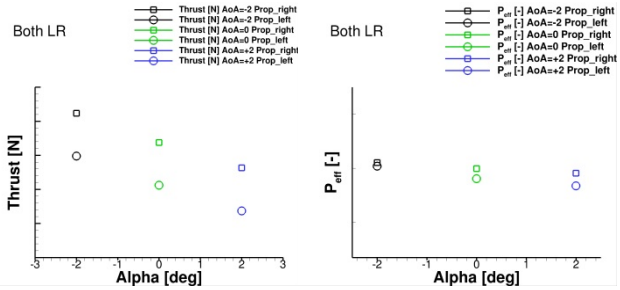

Figure 12 LR average thrust (left) and average power efficiency (right) over AoA with resolved LR and MR interaction

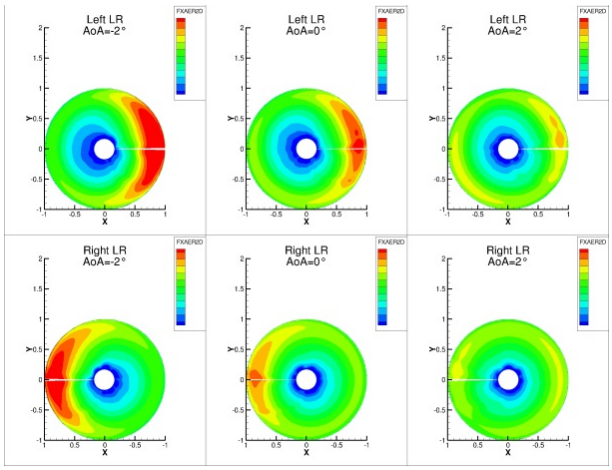

Figure 13 thrust distribution of the LRs for AoA=-2°, AoA=0° and AoA=2° with resolved LR and MR interaction

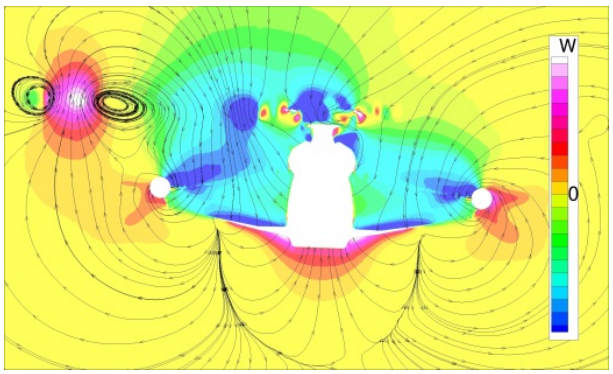

Figure 14 z-component of the flow velocity at constant x plane in front of the LRs

DESIGN OF THE WING SECTION

The aim was to improve the box wing regarding its lift to drag ratio in cruise and its maximum lift capabilities. Therefore, several different approaches were explored by DLR. In a first step the airfoil design was targeted. The second step was to investigate the potential of optimizing the lift distribution of the box wing and at the end the intersections with the fuselage and the lateral rotor nacelles were addressed. Additionally, the wing trim flaps efficiency was evaluated to ensure that the required trim settings could be achieved.

Airfoil

For the airfoil design the minimum thickness is limited by structural strength requirements on the lower wing and by the lateral rotors shaft diameter on the upper wing. Additionally, the maximum chord length was also constrained to avoid an increase of the download factor in hover. This limits the possibilities to improve the airfoils cruise performance significantly. Therefore the focus was set to improve the high lift behavior. The airfoils were first modified in 2-D using X-FOIL, presented in [14]. The most promising results were then verified in 3-D with the TAU-code. With a trailing edge modification, as shown in Figure 15, the maximum lift could be increased. The geometry modification leads to a flow in which the lower trailing edge side flow is more aligned with the upper trailing edge flow, thus decreasing the possibility of separation. Therefore a higher maximum lift can be provided by the modified airfoils. In addition the decreased TE separation tendency is also favorable for positive flap deflection efficiency. Figure 16 shsow that this works quite well on the upper wing for the complete configuration while on the lower wing no significant differences can be observed. This is caused by the increased circulation on the upper wing, reducing the effective AoA of the lower wing and consequently countering the lift increase due to the airfoil modification.

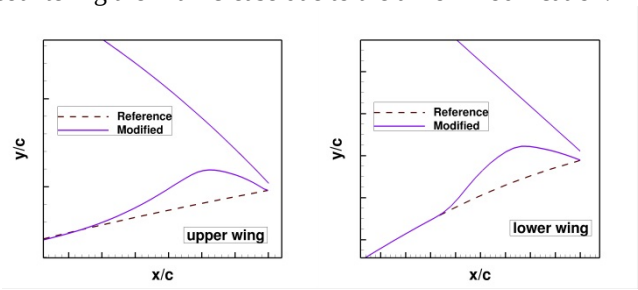

Figure 15 trailing edge modification with lower side cavity to increase lift for the UW (left) and LE (right)

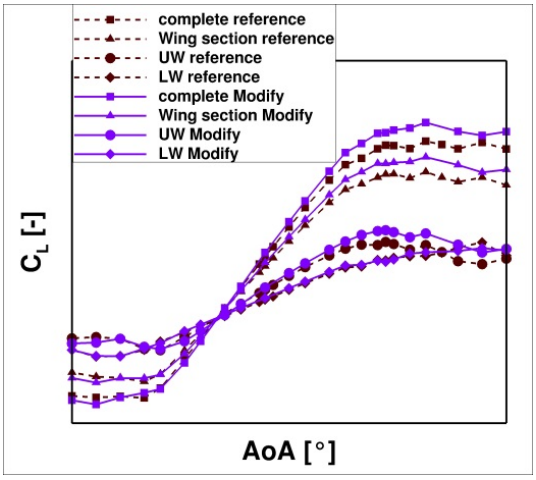

Figure 16 CL over AoA of different parts of the configuration with (purple) and without (dark red) modified airfoils without rotor interaction

Induced box wing drag minimization

In a first step, it was investigated how the box wing induced drag in cruise flight could be reduced by optimizing the circulation distribution. An optimization chain was developed to maximize the spanwise efficiency of box wings and validated with analytical approach of the optimal circulation distribution of a box wing, presented in [15]. Then, the process chain was applied to minimize the induced drag of the upper and lower wings of the RACER configuration. Main and lateral rotor interference was not taken into account at this stage. Figure 17 gives an overview of the process chain. The initial twist design parameters are given as input. These define a twist distribution represented by a B-spline curve. The twist distribution is incorporated into the wing geometry. A surface mesh of the configuration is generated and further preprocessing steps are conducted by a collection of custom python modules. For evaluation of

the aerodynamic performance, the 3D panel code VSAERO, presented in [16] is used. The resulting flow solution is post-processed by an additional python script in order to evaluate the spanwise efficiency factor *e* which is defined as follows:

$$e = \frac{C_L^2}{\pi \Lambda C_D}$$

This factor is used as cost function for an optimizer of the DLR in-house optimization frameworks POT [17] or Pyranha [18]. The optimizers propose a new set of twist design variables until an optimum is found. For this study, a Subplex [19] optimizer was used. This way an optimized circulation distribution was found that improves the efficiency factor *e* by about 51%. The resulting circulation distribution was applied to the configuration by four different approaches with different degree of geometrical complexity. These solutions were recomputed with TAU for verification. As the wings circulation can be manipulated by modifying the twist, the chord and the airfoils, the approaches were defined as follows:

- Nonlinear twist distribution as generated by the VSAERO optimization chain
- Linear twist distribution
- Nonlinear airfoil distribution
- Combination of linear twist and linear chord length distribution

The resulting circulation distributions of the RANS computations at equal lift are presented in Figure 18. The optimization suggests a reduction of the circulation towards the wing tip. To compensate this reduction, the load at the root is increased on both wings. This leads to the best drag reduction of about 6.3% using non-linear twist. The considered alternative approaches return circulation distribution characteristics with variating accuracy, resulting in smaller benefits as it can be observed in Figure 19.

The achieved improvements were also verified taking the main and lateral rotor into account by using actuator discs. As it can be seen in Figure 20, the achieved benefits are significantly reduced. In general, it can be observed that the rotors reduce the gains on the left side, while the benefits of the right wings are increased. This is due to the asymmetrical flow field induced by the main rotor. The relative induced drag benefit is smaller on the left surfaces generating less lift. The drag benefit when considering the rotors is also reduced at the nacelles and the wing tip fairings. This is due to the lateral rotors which are installed counter rotating towards the sense of rotation of the wing tip vortices (clockwise on the right lateral rotor and counter clockwise on the left lateral rotor). This causes the tip vortices to be weakened by the lateral rotor swirl. As the lift distribution optimization gains its drag benefit partially from weakening the tip vortices, the relative benefit towards the reference design is reduced. In conclusion, this confirms that the consideration of the main and lateral rotor interaction during induced wing drag optimization process may lead to better results, when looking at the overall performance of such a complex configuration.

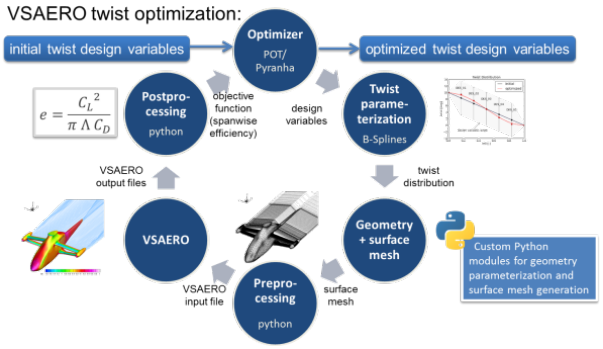

Figure 17 Schema of the circulation distribution optimization chain without rotor interaction

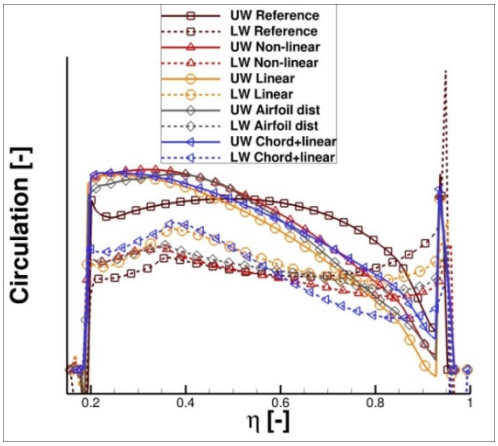

Figure 18 Circulation distribution of the different approaches to fit the result of the optimization chain without rotor interaction

without rotors

	Compl	UW+ LW+ Nacelle	UW right	LW right	Nacelle right	UW left	LW left	Nacelle left	Fuselage
non-linear	-6,29	-10,35	0,81	-2,21	-2,54	0,99	-2,28	-2,53	4,06
linear	-5,27	-10,35	0,36	-1,78	-2,45	0,55	-1,93	-2,44	5,08
airfoil dist	-4,90	-9,69	0,76	-1,16	-2,44	0,23	-1,18	-2,52	4,79
chord+linear	-5,46	-11,81	0,35	-0,78	-2,67	0,61	-0,88	-2,65	6,35

Figure 19 drag benefit breakdown of the different designs without rotor interaction

with rotors

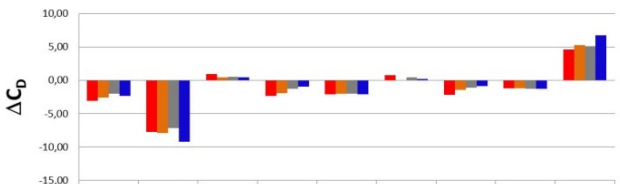

	Compl	UW+ LW+ Nacelle	UW right	LW right	Nacelle right	UW left	LW left	Nacelle left	Fuselage
non-linear	-3,08	-7,76	0,93	-2,28	-2,03	0,78	-2,16	-1,18	4,68
linear	-2,53	-7,85	0,50	-1,92	-1,95	0,08	-1,40	-1,17	5,32
airfoil distl	-2,00	-7,15	0,52	-1,23	-1,98	0,48	-1,10	-1,25	5,15
chord+linear	-2,35	-9,16	0,47	-0,89	-2,05	0,24	-0,82	-1,22	6,81

Figure 20 drag benefit breakdown of the different designs with rotor interaction

Fairings

Due to the box wing design, joined with a nacelle at its tip, the wing has eight intersections (left/right UW/fuselage junction (UWFJ), left/right LW/fuselage junction (LWFJ), left/right UW/nacelle junction (UWNJ) and left/right LW/nacelle junction (LWNJ)). Considering the symmetry of the wing sections the number is reduced to four different junction fairings. These fairings however have different priorities for design.

The UWFJ should be designed to avoid strong flow perturbation at the junction, as the engine intakes are located right above them. This has to be taken into account in the CFD simulation, where the engine intake is simulated by an engine inflow condition with a given mass flow. For the fairing design, several design approaches are studied . Starting from a blunt intersection of the upper wing with the fuselage, the effect of a swept nose device with different sizes was investigated. Additionally, a rounding of the intersection was tested. The drag reduction on the components is summarized in Figure 21. The installation of a swept nose device provides a small drag reduction by reducing the horse-shoe vortex (see Figure 22). This effect increases for a larger nose device and can be further improved by smoothing the intersection of the nose with the wing. A better alternative is to install a rounded fairing. In Figure 22 it can be observed that the horse-shoe vortex is nearly eliminated. A further improvement can be achieved by finding an optimal radius for the rounding leading to a drag reduction of about 2%.

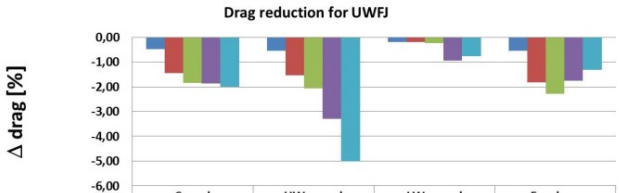

	Compl	UW compl	LW compl	Fuselage
small nose	-0,48	-0,55	-0,20	-0,55
large nose	-1,46	-1,55	-0,19	-1,83
large rounded nose	-1,84	-2,08	-0,25	-2,27
large rounding	-1,88	-3,30	-0,94	-1,75
smaller rounding	-2,01	-5,01	-0,78	-1,31

Figure 21 drag benefit breakdown for the different UWFJ designs without rotor interaction

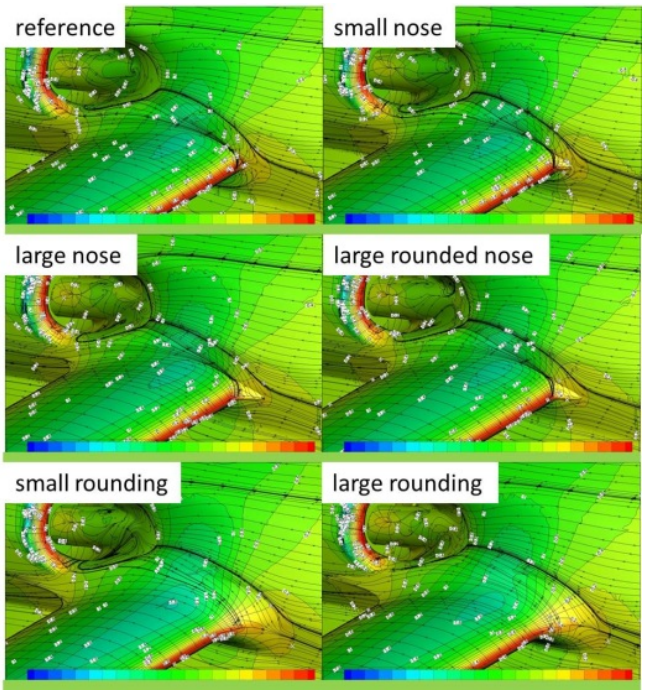

Figure 22 surface solution of the different UWFJ designs without rotor interaction

The LWFJ had to be designed with the aim to reduce the resulting drag on the inboard wing section as well as on the rear of the fuselage. Therefore the installation of a rounding as well as a swept nose device was evaluated. The different considered designs are shown in Figure 23. The impact of the different designs on the components drag is depicted in Figure 24. The installation of a swept nose results in a small benefit for the complete configuration. By reducing the radius of the rounding in the front section, the fairing drag could be significantly improved but to the cost of an increased fuselage drag. The combination of the new design with smaller front radius and the installed swept nose device provides the highest benefit for the complete configuration with about 1.1%.

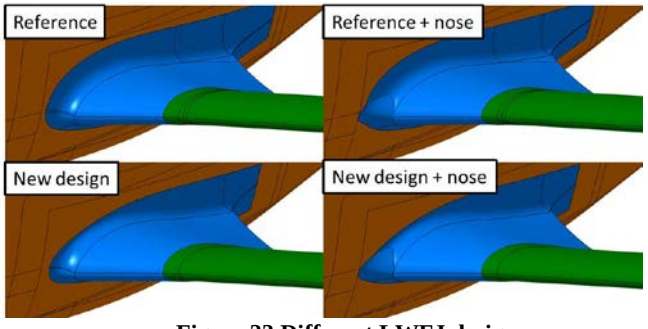

Figure 23 Different LWFJ design

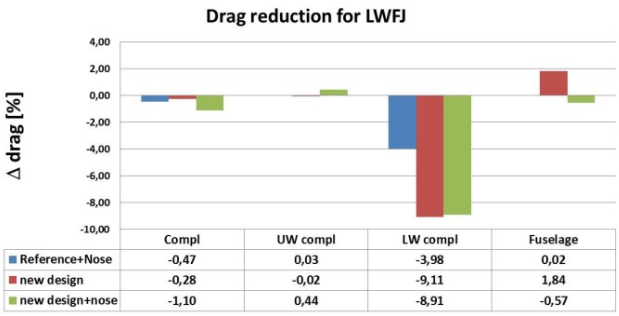

Figure 24 drag benefit breakdown for the different LWFJ designs without rotor interaction

For the nacelle intersection, the UWNJ and LWNJ should provide a best achievable undisturbed flow for the lateral rotors. Therefore the aim was to reduce the horse-shoe vortex and to eliminate all flow separations. Here again the reduction of the horse-shoe vortex is achieved by the installation of swept nose devices.

Because of the lesson learned during the optimization of the circulation distribution, the lateral rotor interaction was taken into account. At this place it was not only important that the lateral rotors have an influence on the wings, but also that the wings have an impact on the lateral rotors performance. To avoid using expensive unsteady RANS computations during the optimization process, the actuator disc approach was used. To consider the wing effect on the lateral rotors, the field solution of the steady state RANS computation without active actuator discs is used as input for the PUMA-code from ONERA. This unsteady free-wake method code evaluates the lateral rotors performance. The computed load distribution is then used for the actuator discs boundaries during a second TAU computation to determine the configuration drag. Figure 25 illustrates the schema used for the coupling of both solvers.

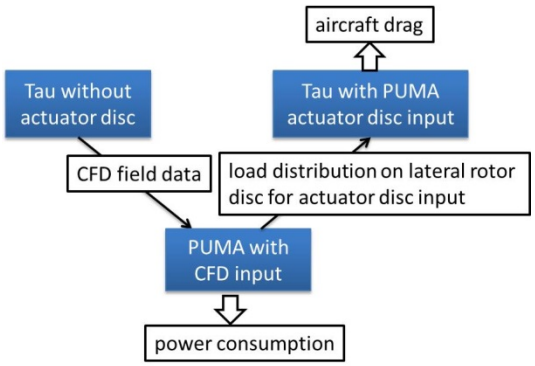

Figure 25 Schema for the coupling of TAU with PUMA for evaluation of the power benefit with lateral rotor interaction

Beside the installation of a swept nose device, two variations of the UWNJ and the LWNJ were assessed. Figure 26 shows the surface solution and the velocity field at the lateral rotors plane for all considered designs. In the lateral rotors plane it can be observed that the disturbances of the horse-shoe vortices of the reference fairings are nearly completely eliminated by the swept nose device of the improved designs. The reference design shows a flow separation on the LWNJ. This could be eliminated by the LWNJ-1 design. Thereby it had to be paid attention that the lateral rotor performance is not negatively affected. This was done by preserving the wing tips load and to even improve it with the UWNJ-1 design. The resulting power balance of the improved fairing designs for drag and lateral rotors power are summarized in Table 2. The UWNJ-1 design returns the smallest benefit in drag power reduction as a small trailing edge separation is provoked. However the high local lift provides a reduction of the power consumption of the lateral rotors. The UWNJ-2 design eliminates the trailing edge separation and consequently the drag power benefit is improved but the lateral rotors efficiency is reduced. This could be compensated by further improvements with the LWNJ-2 design. Thereby the power consumption of the lateral rotors is improved to the cost of smaller drag benefit.

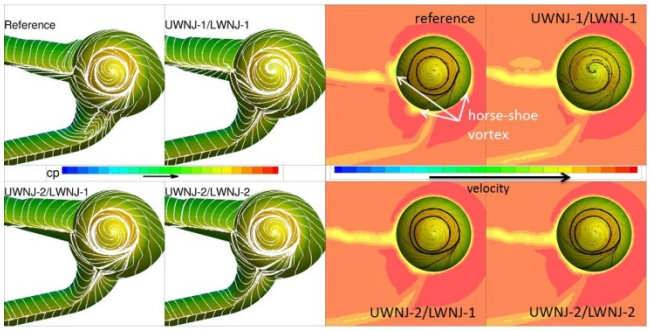

Figure 26 Surface (left) and field solution at the LR plane (right) for different UWNJ and LWNJ with LR interaction

Table 2 power balance for different UWNJ and LWNJ with LR interaction

Fairings UWNJ/LWNJ	ΔP_{drag} [%]	ΔP_{props} [%]	ΔP [%]
UWNJ-1/LWNJ-1	-0.53	-0.35	-0.87
UWNJ-2/LWNJ-1	-0.94	+0.52	-0.42
UWNJ-2/LWNJ-2	-0.82	+0.086	-0.73

Evaluation of flap efficiency (wing)

The RACER configuration design includes flaps at both upper and lower wings and on both the horizontal and vertical stabilizers. They are designed to help trimming the rotorcraft in the various flight states it is supposed to operate in (wing lift adjustment, rolling moment compensation) and to cancel wing lift in autorotation. Simulations were performed in order to check whether the initial sizing fulfills the requirements and to evaluate the efficiency of all wing flaps

The data are to be used to further refine the design and to derive optimal control laws for the wing flaps. Further it is to be clarified if one of the flaps on the upper or lower wing could be preferred or if one of them could be spared. Therefore a high number of computations with different flap setting angle combinations were required. To reduce the computational effort a multi-fidelity surrogate model approach was selected. Therefore the 3D panel code VSAERO was used to provide a low fidelity database with

26x26 samples of differently deflected upper and lower wing flaps. At several points of interest CFD computations with TAU were performed and used as higher fidelity samples. With a thin plate splines (TPS) interpolation approach the data-sets were combined into a surrogate model which computes the flap efficiency for each flap setting combination. Figure 27 shows the lift increase in dependence of the upper and lower wing flap setting angle for the VSAERO samples (left) and for the multi-fidelity surrogate model (right). While for the VSAERO computations the lift production of the flaps is symmetric, the surrogate model shows that the upper wing flap is more efficient to reduce lift while the lower wing flap favorable to increase lift. This gets more evident in Figure 28, where L/D is plotted in dependence of the flap setting angles. For constant lift increase, L/D improves for positive lower wing and negative upper wing flap setting angles. When decreasing the lift, L/D improves by deflecting the upper wing flap in negative direction. In any case one flap is not sufficient to cancel lift. It is necessary to keep both flaps in order to meet the requirements in cruise flight.

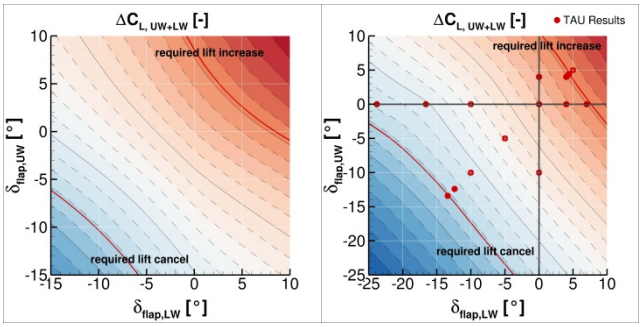

Figure 27 ΔC_L in dependence of the UW and LW flap setting for the VSAERO samples (left) and the multi fidelity surrogate model (right) without rotor interaction

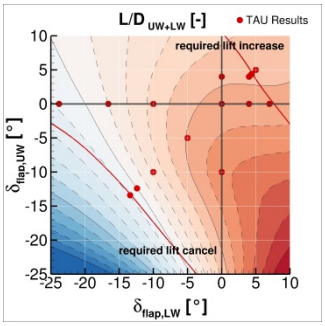

Figure 28 L/D in dependence of the UW and LW flap setting from the multi fidelity surrogate model without rotor interaction

For different flap setting angles of interest, the efficiency in dependence of the aircraft AoA was investigated. The results are presented in Figure 29. For lift augmentation, the deflection of both flaps generates a slightly increased efficiency at higher AoA while the deflection of only the lower wing flap causes a small efficiency loss at higher AoA. At negative AoA the opposite effect can be observed. For the objective of lift cancellation, all considered flap setting combinations have their optimum efficiency at AoA=0°. With changing pitch angles the efficiency for all cases immediatly begin to decrease.

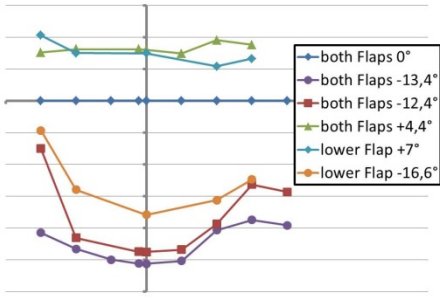

Figure 29 ΔC_L (right) over AoA for different wing flap settings without rotor interaction

DESIGN OF THE HORIZONTAL STABILIZER

Beside the optimization of the wing section, DLR's work was focused on the horizontal stabilizer while the vertical fins are targeted by the core partner ONERA. The target is to improve the longitudinal stability efficiency of the horizontal stabilizer in a wide range of AoA. Due to geometrical and structural constraints, the planform of the horizontal stabilizer was fixed. Therefore only the airfoil and the fairings remain for optimization purposes. Additionally, sufficient trim flap efficiency had to be ensured.

The reference configuration was computed in a wide range of AoA. Repeating these computations for each design iteration with the complete computational mesh would require a high number of CPU hours. Therefore a technique was applied to only compute the flow for the modified tail section without including the frontal components. By using the Dirichlet boundary condition, the airframes wake could be further considered for the tail aerodynamic. The flow conditions for the inflow are extracted from the complete reference configuration computations as shown in Figure 30. This approach assumes that the variations of the empennage have a negligible influence on the front aerodynamic.

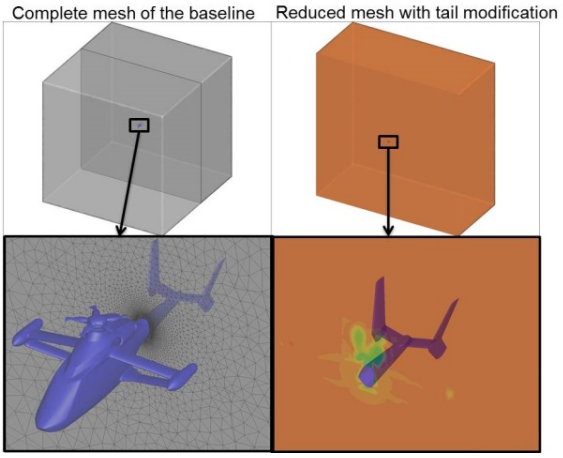

Figure 30 Extraction of the Dirichlet input for the reduced mesh (right) from the complete configuration computation (left)

Horizontal stabilizer airfoil

The horizontal stabilizer airfoil should provide good performance at high positive as well as at high negative AoA. This could be improved by increasing the pressure on both sides with a trailing edge modification as shown in Figure 31. Additionally, the camber was increased and the location of maximum thickness was shifted towards the airfoil nose. In Figure 32 the pitching moment with respect to the rotorcraft center of gravity over AoA and the corresponding gradient are compared for the reference and optimized airfoil. It can be seen that the modifications indeed enable a slightly improved efficiency for higher positive and negative pitch angles. The lift to drag ratio however could not be improved due to the prescribed maximum thickness and the given chord length.

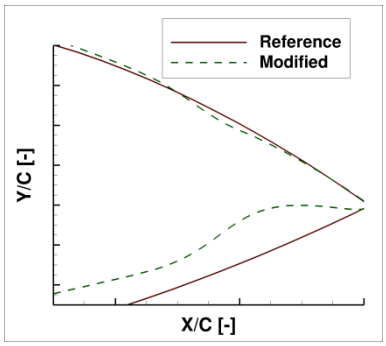

Figure 31 Trailing edge modification on the HS airfoil

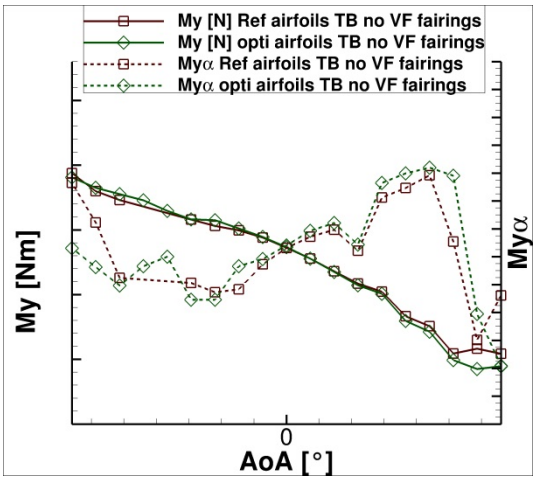

Figure 32 Pitch moment and Myα progression of the empennage

Fairings

In the first investigation of the initial design, it turned out that at the lower side of the HS/VF intersection a massive flow separation occurs. This separation could be removed by an ONERA proposal to give the VFs an X-shape to increase the intersection angle (see Figure 33). At higher negative pitch angle, this location still remains the point of first flow detachments. Therefore the potential of differently sized fairings at the tail boom (TB) intersection and at the vertical fins intersection, presented in Figure 34, are investigated. Figure 35 compares the pitch moment, referred to the rotorcrafts center of gravity and the Myα progressions with and without fairings. The use of a tail boom fairing improves the horizontal stabilizer efficiency for high negative AoA. By adding a fairing at the VF intersection, the pitch moment can be further increased for high positive and negative AoA. In Figure 36 the influence of different sizes of fairings on the My and Myα progression is shown. The variations in size do not generate significant difference in the efficiency of the horizontal stabilizer. Nevertheless, due to the reduced surface, the friction drag is slightly reduced.

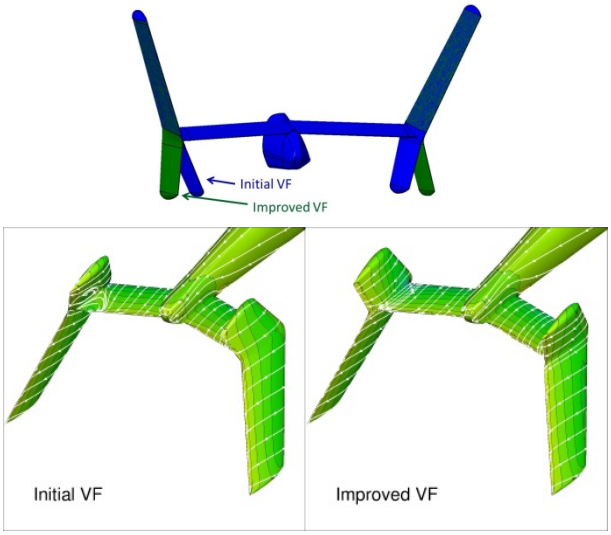

Figure 33 Comparison of initial with improved VF design

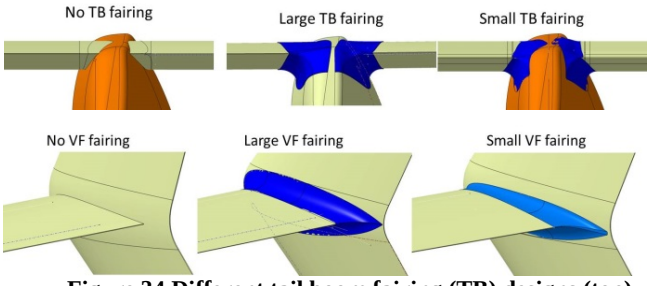

Figure 34 Different tail boom fairing (TB) designs (top) and different vertical fin fairing (VF) designs (bottom)

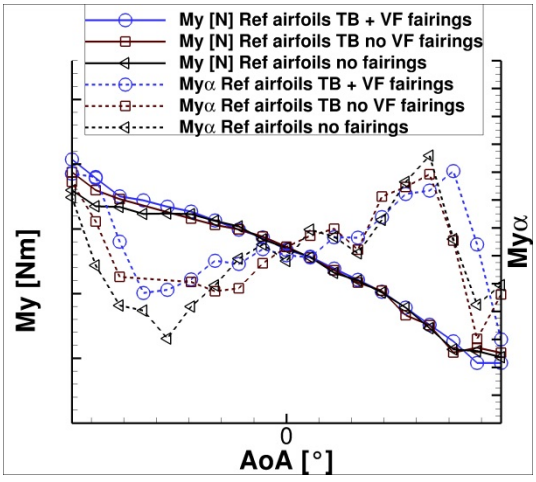

Figure 35 Pitch moment and Myα progression with and without fairings

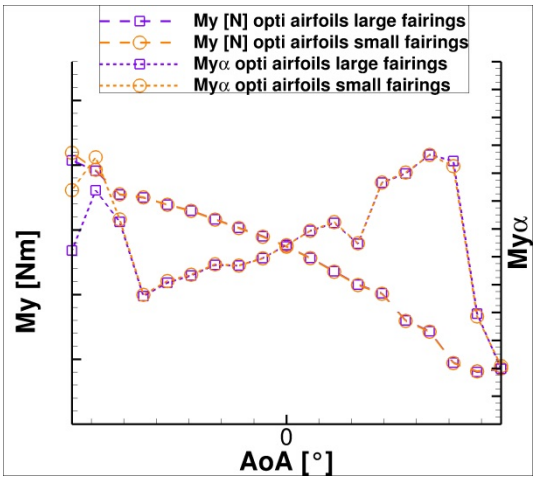

Figure 36 Pitch moment and Myα progression with respect to different size of fairings

Evaluation of flap efficiency (horizontal stabilizer)

For the horizontal stabilizer, it had only to be verified, whether the required maximum trim moments could be achieved with ±5° flap setting angle in a wide range of AoA. The resulting trim moment changes over AoA are plotted in Figure 37. For moderate AoA the maximum target flap deflection is sufficient for the empennage. At high negative AoA a significant drop of the flap efficiency occurs for both flap deflections when the upper deck wake reaches the horizontal stabilizer. For smaller AoA the efficiency recovers again before dropping again due to stall. For positive AoA an increase in the flap efficiency is observed for positive flap deflection, while for negative flap deflection the moment change is reduced. For these AoA the wake of the inboard section of the lower wing hits the empennage and affects its performance. The loss of efficiency for large positive and negative AoA occurs beyond the required range for cruise flight.

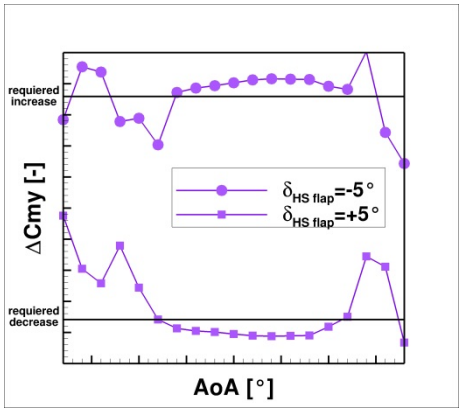

Figure 37 ΔCmy over AoA of the empennage for ±5° HS flap setting angle without rotor interaction

ACOUSTICS EVALUATION

The noise emission from various configurations and several flight conditions were studied for the global acoustic evaluation of the RACER demonstrator. For the purpose of the acoustic evaluation, the aerodynamic tool based on the free wake panel method UPM [8][9][10] is used. UPM is a velocity-based, indirect potential formulation – a combination of source/sink and dipole distribution on the solid surfaces and dipole panels in the wake. The compressibility effect is considered by applying the Prandtl-Glauert correction. UPM has been extended for new compound helicopter configuration and offers an efficient means to predict rotorcraft aerodynamic interaction phenomenon, including all interaction phenomena among main rotor, lateral rotors, fuselage and wings. In the current implementation, the fuselage, tail boom, empennage and nacelle are modeled by a source/sink distribution on the surface. They are not considered as a lifting surface and thus contribute to zero net vorticity to the flow. After a thrust trimmed UPM solution has been obtained, the radiated noise is computed with the Ffowcs-Williams Hawkings (FW-H) solver APSIM [8][9] using the output from UPM.

The complete configuration, as shown in Figure 38, was used in the aerodynamic UPM simulation, so that all interactions among lateral rotors, main rotor, fuselage, wings and tail parts are considered.

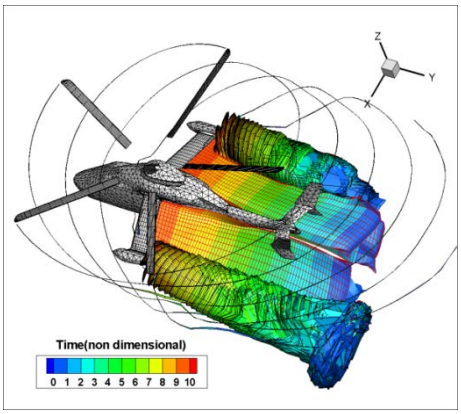

Figure 38 The complete RACER configuration including MR and LRs (for clarity only MR tip vortex is presented), simulation UPM

The flight conditions for acoustics assessment include certification flight cases, such as takeoff and approach in both helicopter (HC) and aircraft (AC) mode. In aircraft mode, the helicopter flies in the same way as a fixed wing airplane and has following characteristics:

- Rotor blades are very close to their own wakes and cut through them; therefore main rotor BVI is expected;
- There is clear distance between main rotor wake and lateral rotor, which indicate that there is no direct main rotor wake/lateral rotor interaction;
- Direct interaction of wing wake with tail parts is observed as shown in Figure 39 (right), which can cause tail parts lift variations.

The comparison of the normal force coefficient computed for the isolated rotor and on the complete configuration is given in Figure 40. The characteristics of aerodynamic BVI at

the advancing and retreating side of the full configuration are similar to that of the isolated rotor (green line). There are almost no changes for major BVI peak positions, which indicate that the influence of the airframe in the rotor wake is very small. In comparison with the isolated rotor the low frequency dynamic loads in 2nd and 3rd quadrant are increased for the complete configuration. It is assumed that the displacement effect of the fuselage and wings is responsible, especially when the rotor blades are pointing toward the upstream direction.

Acoustic assessments on a 150m hemisphere for rotor noise of the complete configuration and the isolated rotor in HC-mode are shown in Figure 41. Similar rotor noise directivities for full and isolated configurations are observed. Slightly reduced maximum levels in noisier area (hot spots) in advancing side for complete configuration are visible, which are also reflected in a slightly reduction of the BVI peak level in Figure 40. In this flight condition, unsteady loading (BVI) noise is dominant and the thickness noise is negligible.

It is thus shown that the BVI phenomena can be captured through the UPM-APSIM evaluation on RACER. Therefore, it is expected to find out and apply low noise command settings which efficiently tackle main rotor BVI, for the specific compound architecture, which allows for an additional Degree-of-Freedom.

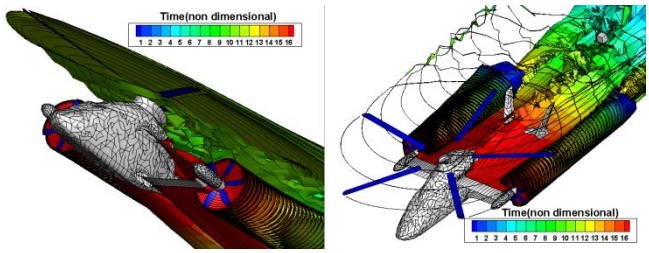

Figure 39 demonstrated the snapshots of wake development in descent HC mode for the complete configuration

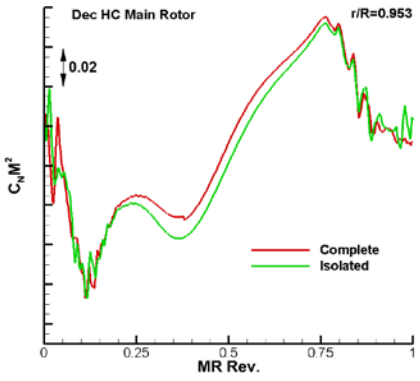

Figure 40 Comparison of CNM2 for descent flight HC mode in two configurations

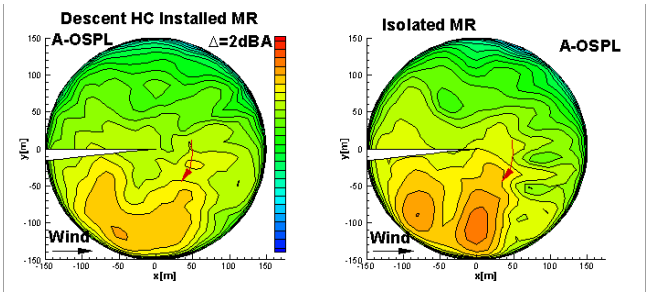

Figure 41 Noise contours from main rotor (red arrow: rotation direction) in complete and isolated configurations on 150m Hemisphere for descent flight HC mode

Due to the special orientation of the lateral rotor, i.e. rotational plane directed towards the ground, it is interesting to divide noise from a lateral rotor into distinct sources, such as thickness (primarily directed in the plane of the lateral rotor) and loading noise. Figure 42 shows an example of the noise radiation of right lateral rotor for the complete configuration. By comparing with overall noise contours (Figure 42 left), the maximum lateral rotor noise is located around rotational plane (thickness noise, Figure 42 middle), while the loading noise (Figure 42 right) is dominant in forward and rearward direction.

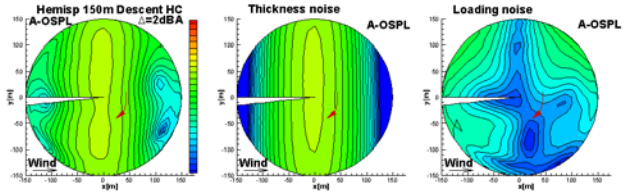

Figure 42 Noise contours from right LR (red arrow: rotation direction) in complete configuration

CONCLUSIONS

DLR was assigned with the task to asses and improve the design of the wing and tail sections of the RACER box wing compound helicopter. The presented studies give an overview of the general aerodynamic characteristics and the resulting interaction phenomena of such a configuration. Out of these insights, different approaches were assessed to improve the RACER cruise speed performance as well as its off design performance at high AoA variations. It was shown that in order to get meaningful results the degree of modeling has to be chosen with care.

First the isolated configuration was evaluated, i.e. without main and lateral rotors interaction, to determine the high AoA properties of the wing and tail section. This was done by using steady state CFD computation with the DLR TAU-code.

By using the TAU transition module, the laminar turbulent transition position on the lifting surfaces was determined. This way the potential of drag reduction and the improved high lift performance of the configuration could be estimated, in case that the noise and vibration level of the

rotorcraft permit the development of a laminar boundary layer.

Beside the isolated investigations, the interference with the main and the lateral rotor is investigated by using actuator discs within the steady state RANS computations. This way, an estimation of the download in hover and the contributions of the different components were evaluated. It was confirmed that the upper wing reduces the lower wing downforce by shadowing it from the main rotor downwash.

During the transition from hover to cruise flight the configuration downforce first increases, before starting to decrease with increasing cruise speed. This is caused by the non-uniform main rotor disc loading resulting in a varying velocity field that passes across the lifting surfaces. At the empennage a similar behavior can be observed, with the difference that for higher speeds, the horizontal stabilizer further produces a downforce.

The rotors interaction on the complete configuration in cruise flight condition causes a reduction of the left wings lift due to the asymmetrical main rotor disc loading. The induced down forces from the main rotor also influence the performance of the lateral rotors. It was further shown that with rising circulation on the wing section, there is an increase in the lateral rotor thrust with constant pitch setting and in the resulting efficiency.

The airfoil design for the wings enables an improved high lift behavior of the RACER configuration. This was achieved by modifying the trailing edge on the pressure side. It seems that the lower wing does not benefit from such a modification. This is due to the fact that the increased circulation of the upper wing counters the additional lift on the lower wing by reducing its effective AoA.

To improve the performance of the wings, a panel method based optimization chain was established to optimize the circulation distribution of the box wing. Applying it to the configuration without rotor interaction, the drag could be reduced by up to 6.2% in cruise flight. However, when considering the rotors, this benefit was approximately halved. Another issue is that by reducing the wing tip load to improve induced drag, the efficiency of the wing tip mounted pusher lateral rotor is decreased. This effect was taken into account during the nacelle fairing optimization. Therefore a tool chain consisting of the DLR TAU-code and the ONERA PUMA code was introduced. Both codes are coupled via the actuator disc in TAU and the field solution in PUMA. With this approach it can be prevented that the gained drag benefit determined by TAU is canceled by the performance losses of the lateral rotors calculated by PUMA. With the applied method it was possible to reduce the overall power consumption for propulsion by about 0.9%. The remaining wing/fuselage fairings are designed to reduce the horse shoe vortex for drag reduction on the lower wing and to prevent flow disturbances for the engine intakes at the upper wing. This could be realized by a swept nose device on the lower wing/fuselage junction and a rounding on the upper wing/fuselage junction.

The different possible combinations of flap settings on the wing section were investigated by using a multi-fidelity surrogate method to reduce the overall CPU time. It turns out, that for lift increase the lower wing flap is more efficient, while for lift decrease the upper wing flap is favorable. However, the installation of both flaps is necessary to enable the required lift cancellation for autorotation phase. The efficiency of the wing and tail flaps is shown to be sufficient within the required AoA range.

The empennage pitch moment efficiency was improved for higher positive and negative AoA by applying a modified airfoil. It was also shown that the installation of rounding fairings at the tail boom and vertical fins intersection further improves the horizontal stabilizer efficiency for higher positive and negative AoA. Neglecting the rotation of the rotor head in the simulations negatively affects the solutions accuracy, especially for the vertical fins, while significantly reducing the computational effort. However it is assumed that the predicted trends are correct and would have to be investigated in further studies.

The acoustic emissions of the configuration are evaluated with the FW-H solver APSIM. The required flow information of the configuration are provided by the unsteady panel code UPM. Using this procedure, the certification flight cases, such as takeoff and approach in both helicopter and aircraft mode were computed for the complete configuration.

The presented study helps to understand the different phenomena of the RACER configuration enabling a capable prototype design.

Author contact: Marc Wentrup Marc.Wentrup@DLR.de
Thorsten Schwarz Thorsten.Schwarz@DLR.de
Philipp Kunze Philipp.Kunze@DLR.de
Thomas Streit Th.Streit@DLR.de
Jianping Yin Jianping.Yin@DLR.de
Jan-Hendrik Wendisch Jan-Hendrik.Wendisch@DLR.de
Jean-Paul Pinacho Jean-Paul.Pinacho@airbus.com
Klaus Kicker Klaus.Kicker@airbus.com
Raphaël Fukari Raphael.Fukari@airbus.com

ACKNOWLEDGMENTS

The authors would like to thank the DLR core partner ONERA for the good, intense and fruitful cooperation. This project has received funding from the European Union's Horizon 2020 research and innovation programme under grant agreement No CS2-AlR-GAM-2014-2015-01.

REFERENCES

[1] M. Blacha, A. Fink, P. Eglin, P. Cabrit "CLEAN SKY2: Exploring New Rotorcraft High Speed Configurations", 43th European Rotorcraft Forum (ERF) 2017, 12-15 September 2017, Milan, Italy

[2] T. Gerhold, "Overview of Hybrid RANS Code TAU", MEGAFLOW – Numerical Flow Simulation for Aircraft Design, edit by N. Kroll and J. Fassbender, Vol. 89 of Notes on Numerical Fluid Mechanics and Multidisciplinary Design, Springer Berlin Heidelberg, 2005, pp. 81-92

[3] D. Schwarmborn, T. Gerhold, R. Heinrich, "The DLR TAU-Code: Recent Applications in Research and Industry", Proceedings of European Conference on Computational Fluid Dynamics ECCOMAS CFD 2006, Delft, Netherlands

[4] D.C. Wilcox, "Reassessment of the Scale-Determining Equation for Advanced Turbulence Models", AIAA Journal, Vol.26, (11), 1988, pp. 1299-1310

[5] Kosorygin V.S., Radeztsky R.H., Saric W.S. "Laminar Boundary-Layer, Sound Receptivity and Control", *Laminar-Turbulent Transition*, edit by Kobayashi R. (eds), IUTAM Symposia (International Union of Theoretical and Applied Mechanics). Springer, Berlin, Heidelberg, 1995, pp. 517–524

[6] G. Schrauf, "LILO 2.1- User's guide and tutorial", 2006, Bericht, Technical Report, GSSC 6, Bremen, Germany

[7] B.Benoit, A.M. Dequin, K. Kampa, W. von Grünhagen, P.M.Basset, B. Gimonet, "HOST, a General Helicopter Simulation Tool for Germany and France", American Helicopter Society, 56th Annual Forum and Technology Display, Virginia Beach, USA, 2000

[8] J. Yin, B.G. van der Wall, G.A. Wilke "Investigation of a simplified aerodynamic modelling technique for noise predictions using FW–H propagation." CEAS Aeronautical Journal, 7 (4), Seiten 551-566. Springer Verlag. DOI: 10.1007/s13272-016-0208-1 ISSN 1869-5582, 2016

[9] J. Yin, B.G. van der Wall, G.A. Wilke "Rotor Aerodynamic and Noise under Influence of Elastic Blade Motion and Different Fuselage Modeling". 40th European Rotorcraft Forum (ERF) 2014, 2-5 September 2014, Southampton, UK.

[10] J. Yin, S.R Ahmed, "Helicopter main-rotor/tail-rotor interaction." Journal of the American Helicopter Society, Vol. 45 (No. 4), Seiten 293-302, 2000

[11] M. Mudry, "La Théorie Générale des Nappes et Filaments Tourbillonnaires et ses Applications à l'Aérodynamique Instationnaire", PhD Thesis Universit´e Paris VI, 1982.

[12] l'Aérodynamique Instationnaire, PhD Thesis Universit´e Paris VI, 1982. D. M. O'Brien, Jr., "Analysis Of Computational Modeling Techniques For Complete Rotorcraft Configurations", Dissertation, Georgia Institute of Technology, May 2006

[13] J.C. Patterson, G.R. Bartlett, "Evaluation of Installed Performance of a Wing Tip Mounted Pusher Turboprop on a Semispan Wing", NACA Technical Paper 2739, 1987

[14] M. Drela, "XFOIL: An Analysis and Design System for Low Reynolds Number Airfoils", University of Notre Dame, Paris, June 1989, Low Reynold Number Aerodynamics, Conference Proceedings,pp. 1-12,1989.

[15] L. Demasi, A. Dipace, G. Monegato, R. Cavallaro, "Invariant Formulation fort the Minimum Induced Drag Conditions of Nonplanar Wing Systems". AIAA Journal. Vol. 52, No. 10, October 2014

[16] J,K, Nathman, "VSAERO – A Computer Program for Calculating the Nonlinear Aerodynamic Characteristics of Arbitrary Configurations. User's Manual, Version 7.2", Analytical Methods, Inc., September 2007

[17] G. Wilke, "Variable Fidelity Optimization of Required Power of Rotor Blades: Investigation of Aerodynamic Models and their Application". In: 38th European Rotorcraft Forum, 2012

[18] J. Brezillon, M. Abu-Zurayk, "Aerodynamic Inverse Design Framework Using Discrete Adjoint Method", Notes on Numerical Fluid Mechanics and Multidisciplinary Design, 121. Springer Verlag. pp. 489-496. January 2013.

[19] T. H. Rowan: "Functional Stability Analysis of Numerical Algorithms", University of Texas at Austin, Diss., 1990